

STELLAR VARIABILITY AT THE MAIN-SEQUENCE TURNOFF OF THE INTERMEDIATE-AGE LMC CLUSTER NGC 1846[†]

R. SALINAS¹, M. A. PAJKOS^{2,7}, A. K. VIVAS³, J. STRADER⁴ AND R. CONTRERAS RAMOS^{5,6}

¹Gemini Observatory, Casilla 603, La Serena, Chile; rsalinas@gemini.edu

²Department of Physics and Astronomy, Butler University, Indianapolis, IN 46208, USA

³Cerro Tololo Interamerican Observatory, National Optical Astronomy Observatory, Casilla 603, La Serena, Chile

⁴Department of Physics and Astronomy, Michigan State University, East Lansing, MI 48824, USA

⁵Millennium Institute of Astrophysics, Av. Vicuña Mackenna 4860, 782-0436 Macul, Santiago, Chile

⁶Instituto de Astrofísica, Pontificia Universidad Católica de Chile, Av. Vicuña Mackenna 4860, 782-0436 Macul, Chile

ABSTRACT

Intermediate-age star clusters in the LMC present extended main sequence turnoffs (MSTO) that have been attributed to either multiple stellar populations or an effect of stellar rotation. Recently it has been proposed that these extended main sequences can also be produced by ill-characterized stellar variability. Here we present Gemini-S/GMOS time series observations of the intermediate-age cluster NGC 1846. Using differential image analysis, we identified 73 new variable stars, with 55 of those being of the Delta Scuti type, that is, pulsating variables close the MSTO for the cluster age. Considering completeness and background contamination effects we estimate the number of δ Sct belonging to the cluster between 40 and 60 members, although this number is based on the detection of a single δ Sct within the cluster half-light radius. This amount of variable stars at the MSTO level will not produce significant broadening of the MSTO, albeit higher resolution imaging will be needed to rule out variable stars as a major contributor to the extended MSTO phenomenon. Though modest, this amount of δ Sct makes NGC 1846 the star cluster with the highest number of these variables ever discovered. Lastly, our results are a cautionary tale about the adequacy of shallow variability surveys in the LMC (like OGLE) to derive properties of its δ Sct population.

Keywords: Magellanic Clouds — globular clusters: individual (NGC 1846) — stars: variables: delta Scuti

1. INTRODUCTION

Intermediate-age (IA) star clusters in the Large Magellanic Cloud (LMC) exhibit extended main sequence turn-offs (MSTOs) inconsistent with single stellar populations (Mackey & Broby Nielsen 2007; Mackey et al. 2008; Milone et al. 2009), which cannot be explained by photometric errors, contamination from the LMC field or binaries (e.g. Goudfrooij et al. 2009). These extended MSTOs can be interpreted as two bursts of star formation separated by a few hundred Myr or a continuous star formation lasting a similar amount of time (Mackey & Broby Nielsen 2007). This interpretation, however, is complicated because any age spread at MSTO level should also be visible at

the red clump, but the morphology of red clumps is rather consistent with single stellar populations (Li et al. 2014; Bastian & Niederhofer 2015, but see Goudfrooij et al. 2015 for a different view). Moreover, for younger clusters with ages of a few Myrs, where any extended star formation should be even clearer in their CMDs, the evidence of departures from single stellar populations remains highly debated (Bastian & Silva-Villa 2013; Correnti et al. 2015; Niederhofer et al. 2015; Milone et al. 2017).

An alternative explanation could be given by stellar rotation. Fast-rotating stars with ages ~ 1.5 Gyr, will have different temperatures as a function of latitude. When viewed from different angles, these temperature differences will be seen as a range of colors and luminosities, producing an extension to the MSTO, mimicking the effect of multiple stellar populations (Bastian & de Mink 2009; Yang et al. 2013; Brandt & Huang 2015), although it has been claimed that rotation alone cannot fully reproduce the extended MSTO morphology (Girardi et al. 2011; Goudfrooij et al. 2017).

Recently, Salinas et al. (2016b) have shown that another previously overlooked factor must be considered

[†]Based on observations obtained at the Gemini Observatory, which is operated by the Association of Universities for Research in Astronomy, Inc., under a cooperative agreement with the NSF on behalf of the Gemini partnership: the National Science Foundation (United States), the National Research Council (Canada), CONICYT (Chile), Ministerio de Ciencia, Tecnología e Innovación Productiva (Argentina), and Ministério da Ciência, Tecnologia e Inovação (Brazil).

⁷CTIO/Gemini REU student.

to understand these extended MSTOs. The instability strip will cross the upper MS and MSTO area for clusters with ages between 1 to 3 Gyr and therefore a certain number of the stars within the instability strip will develop pulsations. These main-sequence pulsators are known as Delta Scuti stars (hereafter δ Sct, see e.g. Breger 2000, for a review). For CMDs obtained using single images per filter, as the great majority of CMDs derived from *HST* images (Mackey & Broby Nielsen 2007; Mackey et al. 2008; Milone et al. 2009), as well as most of the ground-based observations (e.g. Piatti et al. 2014), the act of observing these variables at a random phase means their magnitudes and colors will be away from their static values, producing an artificial broadening of the MSTO that can be misinterpreted as the effect of an extended star formation history or rotation.

The impact of variables near the MSTO will depend on the percentage of stars developing pulsations (the incidence) and on the magnitude of the pulsation amplitudes. These factors are very poorly constrained in extragalactic systems. In Carina, for example, Vivas & Mateo (2013) find a lower limit of 8% for the incidence and an amplitude distribution with a peak at $A_V \sim 0.5$ mag.

The properties of these quantities in the LMC clusters are even less constrained. That is the case because it is difficult to detect them. First, they are faint stars. With magnitudes between 20 and 22 at the LMC distance, they are out of reach of most of the large variability surveys which are conducted with small-aperture telescopes. Second, their periods are short which has a consequence that the exposure times must be kept short to sample correctly the light curve. At least medium size telescopes are needed then.

A quick revision through the catalog of δ Sct in the LMC of Poleski et al. (2010) reveals that for the 14 IA clusters listed in Piatti et al. (2014), between zero and two δ Sct are found per cluster, indicating that crowding significantly hampers the reliability of OGLE at these faint magnitudes, and only a handful of δ Sct have been found in other searches (e.g. Kaluzny & Rucinski 2003).

1.1. The intermediate-age cluster NGC 1846

NGC 1846 (RA=05:07:34.9, Dec=-67:27:32.45) is a rather massive ($M = 1.25 \times 10^5 M_\odot$; Baumgardt et al. 2013), intermediate-age (~ 2 Gyr; Mackey & Broby Nielsen 2007) and metal-rich ([Fe/H]=-0.49; Grocholski et al. 2006) LMC cluster. It was the first LMC cluster where an extended and bifurcated MSTO was detected and firmly established (Mackey & Broby Nielsen 2007; Mackey et al. 2008; Goudfrooij et al. 2009), and where explanations involving field contamination and binary evolution were discarded as a cause (Goudfrooij et al. 2009).

With a core radius of ~ 6.5 pc (Keller et al. 2011), NGC 1846 is also one of the most extended IA clusters, which makes it a more suitable candidate for ground-based photometry. Large core radii have been suggested

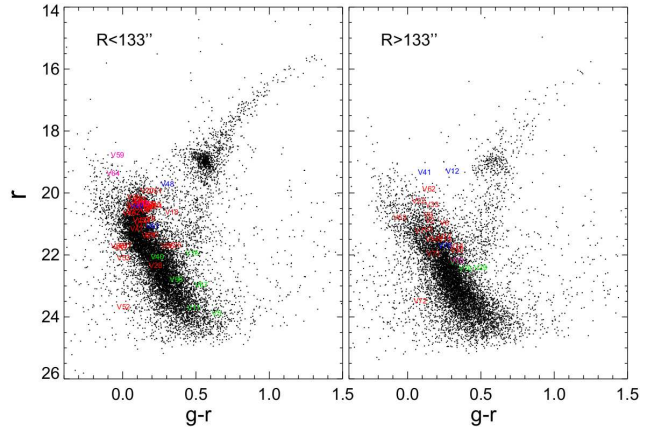


Figure 1. GMOS photometry of the NGC 1846 field. Left panel shows the inner 133'' from the cluster center, while the right panel shows the area outside this limit out to the edges of the GMOS fov. The 133'' limit defines equal areas within the fov. Variable stars discovered in the field are colored according to their classification: delta Scuti (red), RR Lyrae (blue), eclipsing (green) and unknown classification (magenta). The inner population of δ Sct more than doubles the one on the outer field.

to be associated with the presence of extended MSTOs (Keller et al. 2011).

We assess the role of δ Sct in the morphology of the MSTO in IA clusters in the LMC using new time series imaging of the LMC cluster NGC 1846.

2. OBSERVATIONS AND DATA REDUCTION

Observations of NGC 1846 were conducted using the 8.1m Gemini South telescope, located at Cerro Pachón, Chile, on the night of December 30, 2015 under the Gemini Fast Turnaround mode (Gemini program GS-2015B-FT-7). The imaging mode of the Gemini Multi-Object Spectrometer (GMOS, Hook et al. 2004) provided us a 5.5 square arcminute field of view (fov). The SDSS filter system was used to yield 6, 66 and 6 images, in g , r , and i , each having exposure times of 120 s, 120 s, and 90 s, respectively. The total time span of observations was 0.136 days (3.26 hours); adequate for detection of δ Sct which will have periods of less than ~ 6 hours. The GMOS-S array detector consists of three 2048×4176 pixels Hamamatsu detectors, each separated by a gap ~ 30 pixels wide. Observations were obtained with 2×2 binning, resulting in a pixel scale of $0.16''\text{pixel}^{-1}$.

Raw data retrieved from the Gemini Observatory Archive¹, were reduced using the GEMINI package in IRAF². Specifically, the GMOS subpackage allowed us to bias and flatfield correct the raw images, as well as mosaicing the chips and trimming their overscan region. Image quality was measured with the GEMSEEING task.

¹<https://archive.gemini.edu>

² IRAF is distributed by the National Optical Astronomy Observatories, which are operated by the Association of Universities for Research in Astronomy, Inc., under cooperative agreement with the National Science Foundation.

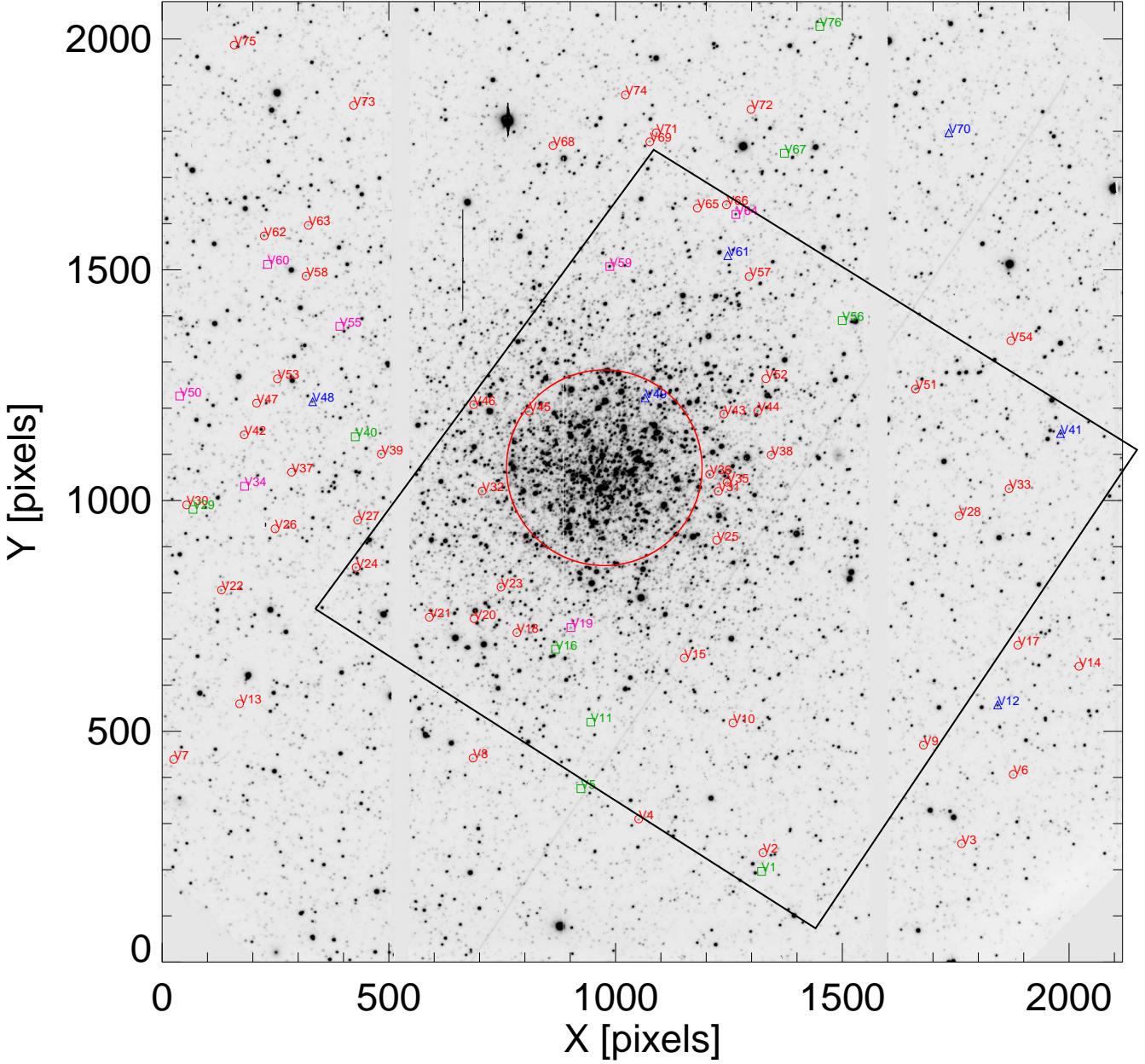


Figure 2. A finder chart for variables in the NGC 1846 field based on a GMOS r image. North is up and East to the left. Positions of δ Sct are indicated with red circles, RRL with blue triangles, eclipsing binaries with green squares. Magenta squares mark the position of variables of unknown type. The central big red circle represents the half-light radius from Goudfrooij et al. (2009). The fov of GMOS is approximately 5.5×5.5 arcmin, while the big black square indicates the HST/ACS pointing used by Goudfrooij et al. (2009) and Milone et al. (2009). North is up, East to the left.

The median FWHM for the r dataset was $0.8''$.

2.1. Photometry

Photometry of the images was obtained using the DAOPHOT/ALLSTAR/ALLFRAME suite of programs developed by Stetson (1987, 1994). As a first step, DAOPHOT was run over all images. The preliminary positions and aperture-photometry magnitudes were

used to obtain the coordinate transformations between the frames with the help of DAOMATCH/DAOMASTER (Stetson 1993). Close to 50 bright isolated stars were visually chosen on the best seeing image of each filter to model the psf as a linearly varying Gaussian profile. The same psf stars were used in the rest of the frames transforming the coordinates using the DAOMASTER output. Once psf-photometry was obtained for all images with

ALLSTAR, a deep reference frame was constructed using the 20 best seeing images. This reference frame was used to obtain the positions of the stars to be measured by ALLFRAME (Stetson 1994), which fits simultaneously the PSF to all stars in all the available images. Final catalogues with mean instrumental magnitudes in g , r and i measured by ALLFRAME were obtained with DAO-MASTER.

Given the absence of standards stars taken on the night of the observations, calibration to the standard system was achieved using the transformation equations provided by the observatory for the Hamamatsu CCDs³.

The color-magnitude diagram of the NGC 1846 field can be seen in Fig. 1. This diagram has further cleaning steps leaving only stars with ALLSTAR parameters $\text{chi} < 10$ and $-2 < \text{sharp} < 2$ and photometric errors less than 0.1 mag in each filter. Photometry of the field is shown split in two equal areas. The left panel shows the inner area ($R < 133''$), where the MSTO of the cluster can be seen at $r \sim 21$ and $g - r \sim 0.15$, and also evidence for old, intermediate and young populations on the LMC field. The subgiant branch of NGC 1846 is barely distinguishable at $r \sim 20$ and $0.2 < g - r < 0.5$. The right panel shows the surrounding field of $R > 133''$. Here the intermediate-age MSTO and red clump are less pronounced and even though a young and intermediate-age population still exist, the dominant feature is the old LMC population, whose MSTO is around $r = 23$. The image quality of ground-based observations does not permit to see the double MSTO, clearly seen with *HST* observations (e.g. Mackey & Broby Nielsen 2007; Milone et al. 2009).

3. VARIABLE STARS IN NGC 1846

3.1. Known variables

We searched for the known variables in the cluster using the on-line search tool provided by OGLE⁴. OGLE lists 44 variables within the field of view observed with GMOS. Of these, 39 are classified as long-period variables, four as RR Lyrae (RRL) and one as Cepheid (Soszyński et al. 2009a,b). No short-period variables were found in this cluster by OGLE. Given the age of the cluster, any RRL or Cepheid will not be a member of the cluster, but members of the LMC field.

3.2. Searching for new variables

New variables stars in the NGC 1846 field were searched using the image subtraction package ISIS (v 2.1, Alard 2000). ISIS first registers images to a common astrometric system. Then a reference frame is constructed as a median from the best seeing images. This reference is then convolved to match the psf of the rest

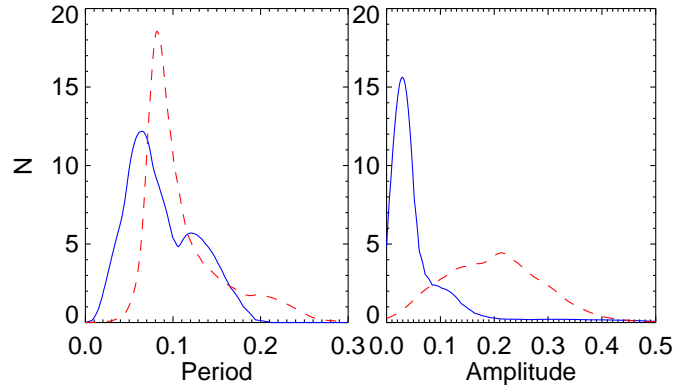


Figure 3. Period (left panel) and amplitude (right panel) distribution of δ Sct in NGC 1846 (blue solid lines) compared to δ Sct in the LMC field from Poleski et al. (2010) (red dashed lines). Note that Poleski et al. (2010) amplitudes are in I while our amplitudes are in r . The bump in the period distribution is an artifact produced by time span limit of the observations.

of the images. Once the psf is matched, the subtraction is applied. This approach leaves in principle only the variable sources as residuals in these subtracted images. ISIS also constructs a variance image as the mean of absolute normalized deviations. This variance image is then visually inspected for meaningful variations in order to discard spurious artifacts produced, for example, around saturated stars (e.g. Salinas et al. 2016a). ISIS finally makes psf photometry on the selected positions where variability is suspected, giving as output light curves in fluxes relative to the reference frame. Variable sources were searched in the r dataset which had the higher cadence of observations. Relative flux light curves are transformed into magnitudes following the procedure from Catelan et al. (2013). Periodicity in the light curves was searched using the phase dispersion minimization algorithm (Stellingwerf 1978) as implemented in IRAF, using as limiting periods 0.001 and 0.3 days

3.3. Variable star classification

The visual inspection of the variance image produced 164 candidate variable sources. Out of this initial list, after a careful visual inspection of the light curves, we settled on 76 genuine varying sources in the NGC 1846 field covered by GMOS. Two of these were not detected by DAOPHOT in either the g nor the r filters due to crowding, and therefore their light curves could not be transformed to magnitudes. Additionally, three more were only detected in the better quality r data. Our final classification, based on the colors, magnitudes, periods, shapes of the light curve and amplitudes of each source, gives as result 55 δ Sct, 8 eclipsing binaries, 5 RRL stars (3 of them already detected by OGLE) and 7 sources with no clear classification.

Table A gives positions, periods and intensity-weighted magnitudes for all these variables. Given the short time span of the observations, for many variables only a lower limit for the period is provided. Phased

³<https://www.gemini.edu/?q=node/10445>

⁴<http://ogledb.astroweb.pl/~ogle/cvs/>

light curves can be seen in Figs. A1 to A4. Additionally, Fig. A5 gives light curves for the candidate and known RRL stars in the field in Julian date versus magnitude. Appendix A also gives notes for some of the variables, especially those with some ambiguity in their classification.

3.4. Period and amplitude distribution

Figure 3 shows the period and amplitude distribution for 48 δ Sct in NGC 1846 where both quantities have been measured, together with the same quantities for 937 δ Sct in the LMC from Poleski et al. (2010). Both distributions were obtained using an adaptive kernel density estimator (Epanechnikov 1969).

The period distribution of δ Sct in NGC 1846 (left panel) has a peak at ~ 0.06 d and a tail towards longer periods. The secondary peak around at ~ 0.13 d is an artifact arising from the time span of the observations, where this lower limit was assigned for δ Sct with longer periods (see Table A). The peak of the period distribution from Poleski et al. (2010) is slightly higher, 0.08d, but significant. The percentage of δ Sct in NGC 1846 with $P < 0.05$ d is 20% while in the Poleski et al. (2010) sample this is only 0.2%. The scarcity of these short-period δ Sct in the Poleski et al. (2010) sample may indicate that the cadence of OGLE observations, close to 3 days (Poleski et al. 2010), is inadequate to find them.

The amplitude distribution of δ Sct in NGC 1846 has its peak around 0.03 mag with a tail towards larger amplitudes up to 0.4 mag. Even though the OGLE data gives amplitudes in the I filter instead of r , it is obvious that the amplitude distribution in the LMC field is very different to the one in NGC 1846. OGLE observations are most likely severely missing a large part of the δ Sct in the LMC field.

4. THE INFLUENCE OF DELTA SCUTI IN THE MSTO MORPHOLOGY

The position of each variable in a CMD can be seen in Fig. 1. As expected, δ Sct cluster around the IA MSTOs of the cluster and the field population, with a few along the upper main sequence, and another group that are probably background δ Sct. Field RRL appear as slightly brighter and redder than the IA TO. The faintness of RRL is partly because all their light curves miss the maximum, making their mean magnitudes dimer.

Fig. 2 in Salinas et al. (2016b) shows that hundreds or even thousands of δ Sct would be needed to produce a significant broadening of the MSTO in IA clusters.

In order to compare with the predictions of Salinas et al. (2016b) we need to estimate the total number of δ Sct in the cluster.

4.1. Artificial stars and completeness

To know how many detections we are missing given crowding and the image quality, we set up a standard artificial stars experiment using the task `addstar` within

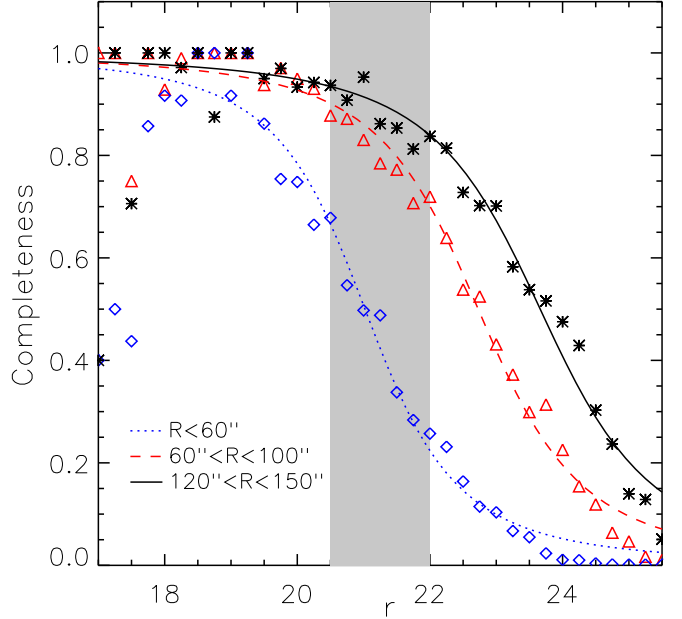


Figure 4. Results from the artificial stars experiment. The different symbols show the completeness at different cluster-centric annuli. The grey stripe highlights the approximate magnitude range that δ Sct will occupy at the cluster's distance.

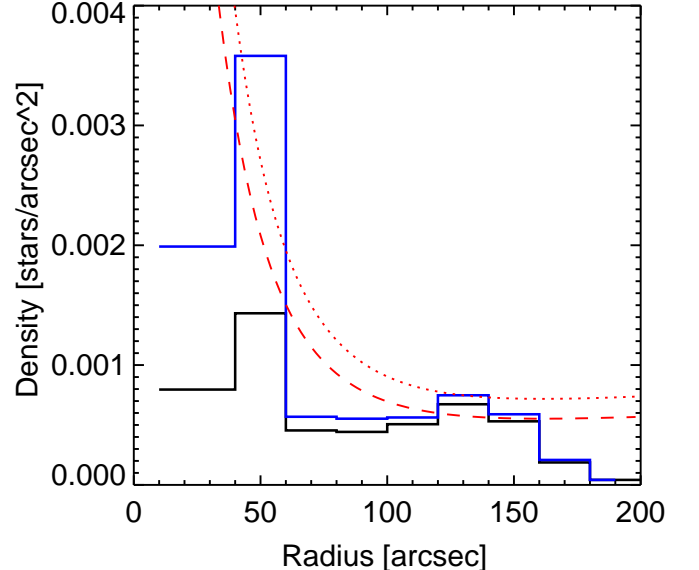


Figure 5. Radial distribution of the discovered δ Sct. The black solid line shows the detected distribution, while the blue line shows the corrected distribution based on the completeness test. The dashed and dotted lines represent the scaled King profiles as described in the text. The estimated numbers for field and cluster δ Sct come from the integration of these King profiles.

DAOPHOT. We added 45 000 artificial stars (in 30 independent runs to avoid overcrowding) with magnitudes between $25 < r < 15$, whose $g - r$ colors and luminosity function were extracted from an IA synthetic CMD produced using BaSTI models (Pietrinferni et al. 2004). Stars were spatially distributed mimicking the distribu-

tion in the field, with 2/3 of the stars in each run randomly distributed and a third with a Gaussian distribution around the cluster center. Once the photometry over the frames with the added stars was done, artificial stars were considered as recovered if they lied within two pixels from their input positions and if the magnitude difference between output and input magnitudes was less than 0.5 mag.

As seen in Fig. 4, completeness is greatly compromised in the inner $\sim 50''$, affecting at the 50% level the $20 < r < 21.5$ magnitude range where most of the δ Sct lie. The completeness is close to 90% for stars outside $\sim 120''$ in the same magnitude range. Lines represent the same interpolating function used e.g. in Salinas et al. (2015).

4.2. Scaling to the total number

Once we know how many δ Sct we are missing as function of radius, we need to use this information to estimate the number of δ Sct in the inner parts of the cluster where the completeness is poor. To this end we assume the incidence of δ Sct will not vary with radius, and that δ Sct follow the same radial distribution as the bright stars that dominate the overall light distribution, that is, there should be no significant mass segregation between the RGB stars and the upper MS stars, given their mass difference of less than $\sim 15\%$. The absence of a strong mass segregation between upper MS stars and RGB stars in NGC 1846 is confirmed by the analysis of Goudfrooij et al. (2009) based on *HST* data.

Goudfrooij et al. (2009) fit the radial distribution of stars in NGC 1846 with a King (1962) profile

$$n(r) = n_0 \left(\frac{1}{\sqrt{1 + (r/r_c)^2}} - \frac{1}{\sqrt{1 + c^2}} \right)^2 + \text{bkg} \quad (1)$$

finding best fit-parameters $n_0 = 8.1$, $r_c = 26''$, $c = 6.2$ and $\text{bkg}=0.267$.

Under the assumption that δ Sct follow the distribution of light, we can scale this profile to find a total number of δ Sct. We use the $120'' < R < 140''$ range to define the normalization of the King profile for the δ Sct. From the completeness experiment (Sec. 4.1), a 90% completeness for δ Sct is expected at this distance. In this annulus there are 11 detected δ Sct. We integrate the King profile between these limits and find a normalization factor of 0.0269 gives the expected number of 12.2 δ Sct in the annulus. Integrating now the King profile from 0 to the tidal radius ($\sim 200''$, Goudfrooij et al. 2009) we obtain 150 δ Sct, where 90 would correspond to the background and 60 would be cluster members.

This number is sensitive to the choice of annulus. If we select instead the $100'' < R < 120''$ range (where we are approximately 80% complete), the same exercise gives us a total number of 45 δ Sct members, which indicates that extrapolations, given our severe inner incompleteness, are necessarily very uncertain. Both King profiles can be seen in Fig. 5.

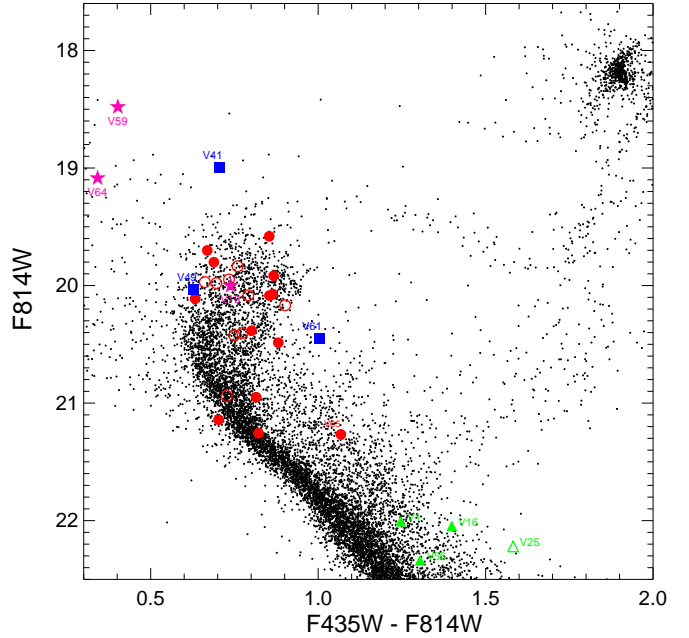


Figure 6. HST photometry of NGC 1846 from Milone et al. (2009) zoomed in the MSTO and upper MS area. 33 of the 36 variable stars found in this paper within the ACS fov are shown. Open symbols represent variables with poor quality photometry as defined in Milone et al. (2009), while filled symbols are variables with good measurements. Red symbols are δ Sct, blue symbols are RRL, green symbols are eclipsing binaries and cyan symbols are variables with undefined class. For clarity only a few δ Sct discussed in the main text are labeled.

Another uncertainty comes from the background level. Structural parameters of NGC 1846 measured by Goudfrooij et al. (2009) using ACS data might overestimate the background given the limited field of view of the ACS. If we assume 90% of the background given by Goudfrooij et al. (2009) then the total number of δ Sct increases to a range between 50 and 65. At 70% of the background, this range increases to 62 and 84.

4.3. A comparison with *HST* photometry

Even though the number of discovered δ Sct, their estimated total amount, and in general the low amplitudes found are most likely not enough to produce any significant broadening of the MSTO, it is interesting to see what impact these discovered δ Sct have in the published *HST* photometry.

We cross-matched the F435W/F814W *HST*/ACS photometry of NGC 1846 from Milone et al. (2009) to the positions of our discovered variables. Given the much smaller ACS fov, only 35 of the discovered variables are found within this fov; 25 being δ Sct. These can be seen as red symbols in Fig. 6. Catalogues were matched using a combination of CATACOMB⁵ and STILTS (Taylor 2006).

⁵ Developed by Paolo Montegriffo at the Bologna Astronomical Observatory

Just like in the case of the GMOS photometry (Fig. 1), variables stars concentrate at the MSTO. Fig. 6 shows the ACS photometry of the upper MS and MSTO areas where 32 of the discovered variables stars are. Open symbols are stars with poorly measured photometry according to Milone et al. (2009) based on the frame-to-frame scatter (see below), uncertainty in the frame-to-frame position and the residual of the psf fit.

One notable feature is that δ Sct do not lie preferentially along any of the split sequences, but instead scatter along both and with slightly larger range in color, as expected for variable stars caught at a random phase.

The Milone et al. (2009) ACS photometry of NGC 1846 comes from 3 exposures in F435W and 4 in F814W. Despite that Milone et al. (2009) applied a selection based on the rms of the magnitudes in different exposures to set up the good quality sample, 24 out of the 35 variables were labeled as good quality by them, including all 3 RRL which are expected to have the largest rms based on their larger amplitudes. This again proves the inadequacy of using poorly time-sampled data, as is the case of all IA LMC clusters observed with *HST*, in order to detect variable stars.

5. SUMMARY AND CONCLUSIONS

In this paper we explored the influence the δ Sct pulsators have in the morphology of the MSTO in IA clusters in the LMC. Since the great majority of the photometry of these clusters comes from using merely 1 or 2 images per filter (e.g. Mackey & Broby Nielsen 2007; Milone et al. 2009; Piatti et al. 2014), these variables have so far being undetected, and their role ignored.

Using new time series photometry of the LMC IA cluster NGC 1846 obtained with Gemini South, we have discovered 55 δ Sct in the field of NGC 1846, plus 18 variables of other types. This is the first in-depth study of the short-period variables in an LMC cluster. Considering completeness and background contamination we estimate the number of δ Sct belonging to the cluster somewhere around 40 and 60. This number of δ Sct will not produce a significant impact in the MSTO morphology, as hundreds or even thousands would be needed to produce a significant broadening of the MSTO according to the modelling of Salinas et al. (2016b).

This estimated total number of δ Sct is still very uncertain. We assumed the radial distribution of δ Sct follows the light of the cluster to extrapolate the density of

δ Sct to the inner radii where crowding makes measurements impossible. Moreover, we detected only one δ Sct within the half-light radius, where a large number of variables should still be uncovered. Only time-series observations with higher spatial resolution will provide the final answer to the role δ Sct have in the broadening of MSTOs.

Finally, we note that NGC 1846 is, to our knowledge, the star cluster with the largest population of δ Sct ever discovered, including open clusters in our Galaxy (e.g. Andersen et al. 2009; Sandquist et al. 2016). This opens new avenues for the study of PL relations of δ Sct, for example, as function of metallicity, that will be studied in a forthcoming paper. The fact that we have discovered more than 50 of these variables in a patch of the sky where OGLE detected none, is a warning that OGLE is most probably severely incomplete for fields with only mild crowding, and very biased towards variables with long periods and large amplitudes; therefore probably thousands of δ Sct, fainter, mostly eclipsing, variables and even some RRL located in the distant edge of the LMC, remain to be discovered.

We thank the anonymous referee for a fast report which helped us clarify several issues. RS thanks Antonino Milone for making his *HST*/ACS photometry of NGC 1846 available and Ernst Paunzen for pointing us to the Galactic clusters richest in δ Sct. We thank Catherine Kaleida for all her efforts organizing the REU program at CTIO. This project was conducted in the framework of the CTIO REU Program, which is supported by the National Science Foundation under grant AST-1062976. JS acknowledges partial support from NSF grant AST-1308124 and the Packard Foundation. Based on observations made with the NASA/ESA Hubble Space Telescope, and obtained from the Hubble Legacy Archive, which is a collaboration between the Space Telescope Science Institute (STScI/NASA), the Space Telescope European Coordinating Facility (ST-ECF/ESA) and the Canadian Astronomy Data Centre (CADC/NRC/CSA).

Facility: Gemini-S

Software: IRAF (Tody 1986, 1993), ISIS (v 2.1, Alard 2000), CataComb, stilts (Taylor 2006), daophot/allstar/allframe (Stetson 1987, 1994), daomatch/daomaster (Stetson 1993)

REFERENCES

- Alard, C. 2000, A&AS, 144, 363
- Andersen, M. F., Arentoft, T., Frandsen, S., et al. 2009, Communications in Asteroseismology, 160, 9
- Bastian, N., & de Mink, S. E. 2009, MNRAS, 398, L11
- Bastian, N., & Niederhofer, F. 2015, MNRAS, 448, 1863
- Bastian, N., & Silva-Villa, E. 2013, MNRAS, 431, L122
- Baumgardt, H., Parmentier, G., Anders, P., & Grebel, E. K. 2013, MNRAS, 430, 676
- Brandt, T. D., & Huang, C. X. 2015, ApJ, 807, 25
- Breger, M. 2000, in Astronomical Society of the Pacific Conference Series, Vol. 210, Delta Scuti and Related Stars, ed. M. Breger & M. Montgomery, 3
- Catelan, M., Minniti, D., Lucas, P. W., et al. 2013, in 40 Years of Variable Stars: A Celebration of Contributions by Horace A. Smith (ed. K. Kinemuchi et al.), 139, arXiv:1310.1996

- Correnti, M., Goudfrooij, P., Puzia, T. H., & de Mink, S. E. 2015, MNRAS, 450, 3054
- Epanechnikov, V. A. 1969, Teor. Veroyatnost. i Primenen., 14
- Girardi, L., Eggenberger, P., & Miglio, A. 2011, MNRAS, 412, L103
- Goudfrooij, P., Girardi, L., & Correnti, M. 2017, ApJ, 846, 22
- Goudfrooij, P., Girardi, L., Rosenfield, P., et al. 2015, MNRAS, 450, 1693
- Goudfrooij, P., Puzia, T. H., Kozhurina-Platais, V., & Chandar, R. 2009, AJ, 137, 4988
- Grocholski, A. J., Cole, A. A., Sarajedini, A., Geisler, D., & Smith, V. V. 2006, AJ, 132, 1630
- Hook, I. M., Jørgensen, I., Allington-Smith, J. R., et al. 2004, PASP, 116, 425
- Kaluzny, J., & Rucinski, S. M. 2003, AJ, 126, 237
- Keller, S. C., Mackey, A. D., & Da Costa, G. S. 2011, ApJ, 731, 22
- King, I. 1962, AJ, 67, 471
- Li, C., de Grijs, R., & Deng, L. 2014, ApJ, 784, 157
- Mackey, A. D., & Broby Nielsen, P. 2007, MNRAS, 379, 151
- Mackey, A. D., Broby Nielsen, P., Ferguson, A. M. N., & Richardson, J. C. 2008, ApJL, 681, L17
- Milone, A. P., Bedin, L. R., Piotto, G., & Anderson, J. 2009, A&A, 497, 755
- Milone, A. P., Marino, A. F., D'Antona, F., et al. 2017, MNRAS, 465, 4363
- Niederhofer, F., Hilker, M., Bastian, N., & Silva-Villa, E. 2015, A&A, 575, A62
- Piatti, A. E., Keller, S. C., Mackey, A. D., & Da Costa, G. S. 2014, MNRAS, 444, 1425
- Pietrinferni, A., Cassisi, S., Salaris, M., & Castelli, F. 2004, ApJ, 612, 168
- Poleski, R., Soszyński, I., Udalski, A., et al. 2010, AcA, 60, 1
- Salinas, R., Alabi, A., Richtler, T., & Lane, R. R. 2015, A&A, 577, A59
- Salinas, R., Contreras Ramos, R., Strader, J., et al. 2016a, AJ, 152, 55
- Salinas, R., Pajkos, M. A., Strader, J., Vivas, A. K., & Contreras Ramos, R. 2016b, ApJL, 832, L14
- Sandquist, E. L., Jessen-Hansen, J., Shetrone, M. D., et al. 2016, ApJ, 831, 11
- Soszyński, I., Udalski, A., Szymański, M. K., et al. 2009a, AcA, 59, 1
- . 2009b, AcA, 59, 239
- Stellingwerf, R. F. 1978, ApJ, 224, 953
- Stetson, P. B. 1987, PASP, 99, 191
- Stetson, P. B. 1993, in IAU Colloq. 136: Stellar Photometry - Current Techniques and Future Developments, ed. C. J. Butler & I. Elliott, 291
- . 1994, PASP, 106, 250
- Taylor, M. B. 2006, in Astronomical Society of the Pacific Conference Series, Vol. 351, Astronomical Data Analysis Software and Systems XV, ed. C. Gabriel, C. Arviset, D. Ponz, & S. Enrique, 666
- Tody, D. 1986, in Proc. SPIE, Vol. 627, Instrumentation in astronomy VI, ed. D. L. Crawford, 733
- Tody, D. 1993, in Astronomical Society of the Pacific Conference Series, Vol. 52, Astronomical Data Analysis Software and Systems II, ed. R. J. Hanisch, R. J. V. Brissenden, & J. Barnes, 173
- Vivas, A. K., & Mateo, M. 2013, AJ, 146, 141
- Yang, W., Bi, S., Meng, X., & Liu, Z. 2013, ApJ, 776, 112

APPENDIX

A. NOTES ON SOME INDIVIDUAL VARIABLES

V1: even though this could easily be an eclipsing variable at the MSTO of the old LMC population, its curve at maximum light also resembles a RRc variable.

V5: by its color and luminosity is most probably a MS contact binary, although its shape looks more sawtooth-like than sinusoidal.

V12: according to [Soszyński et al. \(2009a\)](#), this is RRL OGLE-LMC-RRLYR-05278 with period 0.5870247d.

V19: has the magnitude and color of cluster δ Sct, but its shape does not resemble a δ Sct, therefore we classify it as unknown type.

V25: this is a very faint source for which we do not have psf photometry and therefore the light curve cannot be transformed into magnitudes. We originally classified this variable as δ Sct based on its shape and period, but its position in the *HST* CMD (Fig. 6), reveals it as a more likely eclipsing binary.

V34: another very faint source, for which we lack color information. Its light curve resembles more a δ Sct than a eclipsing binary, therefore is probably a background source.

V41: according to [Soszyński et al. \(2009a\)](#), this the RRe (second-overtone pulsator) OGLE-LMC-RRLYR-05379 with a period of 0.272447d

V48: this is OGLE-LMC-RRLYR-05394 from [Soszyński et al. \(2009a\)](#), with period 0.472163 d.

V49: even though it has a magnitude and color that puts it right at the MSTO, its period is much longer than the timespan of the observations. Even though it could be a δ Sct with a very long period, it is more likely a background RRL that was not discovered by OGLE.

V50: another source without color. Shape of light curve and period indicate a δ Sct, although its faintness implies a background source. With $A_r=0.5$ is one of the variables with the largest amplitudes in the sample.

V52: has the color of a δ Sct, but a much fainter magnitude. Probably a background δ Sct.

V53: a δ Sct appearing about a magnitude below the MSTO. Most likely a LMC field δ Sct somewhat on the background.

V55: another variable too faint in g to obtain a color. It is very faint in i , but has an amplitude ~ 0.5 mag. Its light curve shape resembles a δ Sct an a RRL, but we cannot adventure any firm classification.

V56: Most probably a long period eclipsing binary.

V57: similar to V53.

V59: the brightest of all variables, but with a very small amplitude to be a RRL. We cannot determine a classification for this variable.

V60: too faint and red to be a δ Sct. We set its class as Unknown.

V61: has the right magnitude and color to be a δ Sct in NGC 1846, but its very high amplitude and rather long period points at a background RRL.

V64: is one of the bluest variables in the sample. Brighter than the MSTO, its partial light curve resembles the sinusoidal shape of a RRc, although that would be a very tentative classification.

V68: like V53 and V 57, this variable appears below the MSTO of NGC 1846. Is probably a background δ Sct.

V70: the partial shape of this light curve hints at a background RRL.

V72: same as V52.

V75: another variable for which we could not transform relative flux into magnitudes. Its short period and light curve shape indicate is a δ Sct.

Table A1. Positions, mean magnitudes, r amplitudes, periods and classification for all the variables discovered in the NGC 1846 field. Uncertain amplitudes are indicated with a colon, while the $>$ indicates lower limits for some periods. The classification is D: delta Scuti, RRL: RR Lyrae, E: eclipsing binary, LP: long period variable, and U: variable with unknown classification. The last column indicates either a cross identification with OGLE or a note in Sect. A indicated with the * sign.

ID	RA (J2000)	Dec (J2000)	$\langle g \rangle$	$\langle r \rangle$	A_r	$P(d)$	Type	Note
V1	05:07:10.061	-67:28:34.35	22.60	22.31	0.31	0.17	E	*
V2	05:07:11.184	-67:28:34.85	21.10	20.98	0.03	0.042	D	
V3	05:07:11.684	-67:29:44.91	21.37	21.26	0.02	0.043	D	
V4	05:07:13.242	-67:27:51.07	20.78	20.66	0.02	0.076	D	
V5	05:07:15.079	-67:27:30.68	24.58	23.97	0.32	0.13	E	*
V6	05:07:15.856	-67:30:03.18	21.27	21.05	0.03:	0.14	D	
V7	05:07:16.925	-67:25:07.09	21.35	21.30	0.10	0.060	D	
V8	05:07:16.946	-67:26:52.67	21.06	20.90	0.04	0.064	D	
V9	05:07:17.633	-67:29:31.52	20.90	20.79	0.03	0.075	D	
V10	05:07:19.007	-67:28:24.38	21.57	21.42	0.02	0.052	D	
V11	05:07:19.084	-67:27:34.23	24.23	23.79	0.25:	> 0.15	E	
V12	05:07:20.048	-67:29:57.74	19.64	19.38	0.10:	> 0.2	RRL	OGLE-LMC-RRLYR-05278
V13	05:07:20.256	-67:25:30.38	21.80	21.59	0.08	0.042	D	
V14	05:07:22.364	-67:30:26.48	22.09	21.80	0.03	0.15	D	
V15	05:07:22.941	-67:28:07.24	21.02	20.95	0.04	0.076	D	
V16	05:07:23.480	-67:27:21.83	22.44	22.01	0.18	0.13	D	
V17	05:07:23.651	-67:30:04.94	21.69	21.48	0.03	0.054	D	
V18	05:07:24.485	-67:27:08.23	20.98	20.69	0.03	0.14	D	
V19	05:07:24.787	-67:27:27.30	20.51	20.42	0.04:	> 0.14	U	*
V20	05:07:25.334	-67:26:53.16	20.12	20.00	0.02	0.1	D	
V21	05:07:25.431	-67:26:37.37	21.59	21.46	0.05	0.10	D	
V22	05:07:27.099	-67:25:24.06	20.36	20.33	0.03:	0.12	D	
V23	05:07:27.237	-67:27:02.63	20.35	20.28	0.04	0.068	D	
V24	05:07:28.438	-67:26:11.55	20.69	20.51	0.03:	0.10	D	
V25	05:07:30.025	-67:28:18.75	—	—	—	0.13	E	*
V26	05:07:30.772	-67:25:42.96	22.07	21.76	0.06	0.046	D	
V27	05:07:31.283	-67:26:12.13	20.49	20.46	0.01	0.044	D	
V28	05:07:31.454	-67:29:44.21	22.59	22.41	0.09	0.046	D	
V29	05:07:31.953	-67:25:14.02	22.94	22.49	0.12:	> 0.12	E	
V30	05:07:32.221	-67:25:11.77	22.22	21.93	0.08	0.15	D	
V31	05:07:32.974	-67:28:19.35	20.51	20.42	0.02	0.074	D	
V32	05:07:33.023	-67:26:56.07	20.55	20.43	0.04	0.078	D	
V33	05:07:33.096	-67:30:01.91	20.57	20.45	0.20:	0.11	D	
V34	05:07:33.336	-67:25:32.26	—	24.09	0.25	0.12	U	*
V35	05:07:33.519	-67:28:22.44	20.57	20.44	0.08	0.12	D	
V36	05:07:34.001	-67:28:16.31	20.24	20.21	0.02	0.078	D	
V37	05:07:34.180	-67:25:48.84	21.74	21.77	0.13	0.14	D	
V38	05:07:35.155	-67:28:38.01	20.70	20.59	0.03	0.125	D	
V39	05:07:35.255	-67:26:20.48	20.39	20.33	0.02	0.071	D	
V40	05:07:36.298	-67:26:11.30	22.33	22.14	0.10	0.14	E	
V41	05:07:36.410	-67:30:20.05	19.49	19.42	0.07:	> 0.16	RRL	OGLE-LMC-RRLYR-05379
V42	05:07:36.430	-67:25:32.14	20.73	20.70	0.02	0.038	D	

Table A1 continued

Table A1 (*continued*)

ID	RA (J2000)	Dec (J2000)	$\langle g \rangle$	$\langle r \rangle$	A_r	$P(d)$	Type	Note
V43	05:07:37.626	-67:28:21.32	20.63	20.50	0.02	0.095	D	
V44	05:07:37.799	-67:28:33.29	20.47	20.39	0.10	0.075	D	
V45	05:07:37.816	-67:27:12.63	20.63	20.46	0.03	0.104	D	
V46	05:07:38.220	-67:26:53.09	20.74	20.74	0.04	0.071	D	
V47	05:07:38.335	-67:25:36.50	21.29	21.24	0.08:	> 0.20	D	
V48	05:07:38.412	-67:25:56.26	20.06	19.80	0.08:	> 0.16	RRL	OGLE-LMC-RRLYR-05394
V49	05:07:38.618	-67:27:53.52	20.55	20.50	0.16:	> 0.2	RRL	*
V50	05:07:38.767	-67:25:09.38	—	24.44	0.50	0.10	U	*
V51	05:07:39.109	-67:29:28.91	20.20	20.02	0.02	0.15	D	
V52	05:07:39.754	-67:28:36.16	23.72	23.76	0.40	0.071	D	*
V53	05:07:39.796	-67:25:43.87	22.13	22.17	0.15	0.16	D	*
V54	05:07:42.020	-67:30:02.59	21.68	21.56	0.02	0.049	D	
V55	05:07:42.945	-67:26:05.89	—	23.42	0.50:	> 0.1	U	*
V56	05:07:43.251	-67:29:03.09	23.19	22.87	0.25:	> 0.15	E	*
V57	05:07:45.914	-67:28:30.28	21.80	21.86	0.05	0.049	D	*
V58	05:07:45.974	-67:25:53.99	20.51	20.47	0.03	0.11	D	
V59	05:07:46.526	-67:27:41.14	18.78	18.86	0.01	> 0.16	U	*
V60	05:07:46.679	-67:25:40.43	22.55	22.26	0.11	> 0.10	U	*
V61	05:07:47.170	-67:28:22.70	21.31	21.15	0.80:	> 0.2	RRL	*
V62	05:07:48.396	-67:25:39.26	20.05	19.95	0.11	0.09	D	
V63	05:07:49.025	-67:25:54.81	20.77	20.87	0.12	0.07	D	
V64	05:07:49.655	-67:28:25.60	19.34	19.45	0.01:	> 0.16	U	*
V65	05:07:50.038	-67:28:11.99	22.05	21.79	0.06	> 0.16	D	
V66	05:07:50.236	-67:28:22.26	20.57	20.55	0.01	0.047	D	
V67	05:07:53.337	-67:28:42.72	23.53	23.04	0.35	0.11	E	
V68	05:07:53.811	-67:27:21.08	21.72	21.80	0.12:	> 0.16	D	*
V69	05:07:54.035	-67:27:55.26	20.65	20.54	0.02	0.127	D	
V70	05:07:54.560	-67:29:40.68	21.98	21.77	0.12:	> 0.2	RRL	*
V71	05:07:54.581	-67:27:57.52	21.16	21.08	0.02	0.067	D	
V72	05:07:55.982	-67:28:30.90	23.61	23.57	0.34	0.128	D	*
V73	05:07:56.233	-67:26:10.71	22.16	22.03	0.05	0.15	D	
V74	05:07:56.857	-67:27:46.59	21.06	20.96	0.02	0.057	D	
V75	05:07:59.875	-67:25:28.64	—	—	—	0.095	D	*
V76	05:08:00.985	-67:28:55.19	22.88	22.53	0.12:	> 0.18	E	

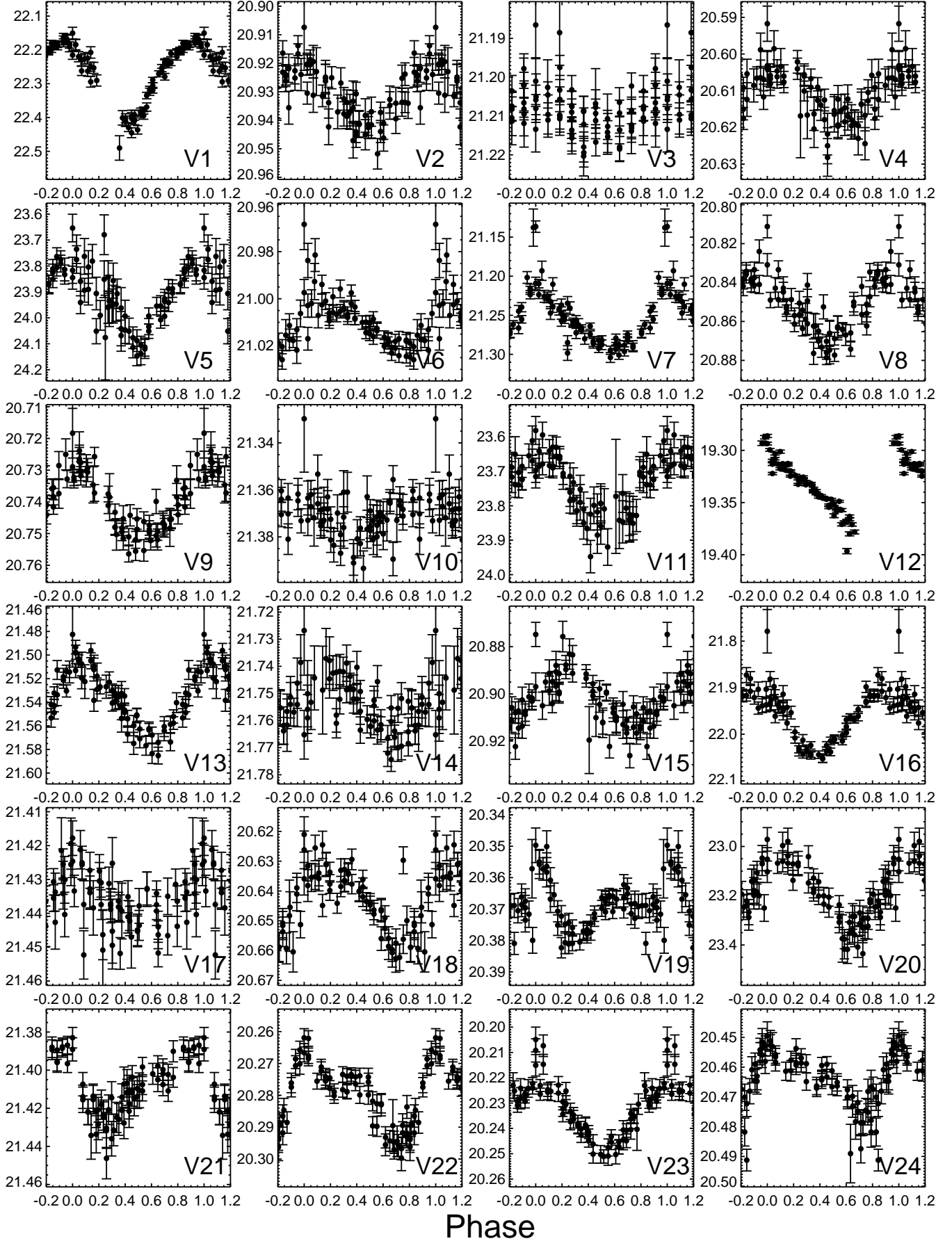


Figure A1. Folded light curves of all the new variables stars in the NGC 1846 field. All light curves were measured in the r band. Note that a couple of them (V25 and V75) were not calibrated into standard magnitudes and their light curve are only shown in relative counts. Variables where only a minimum period is given in Table A, were phased using this minimum period.

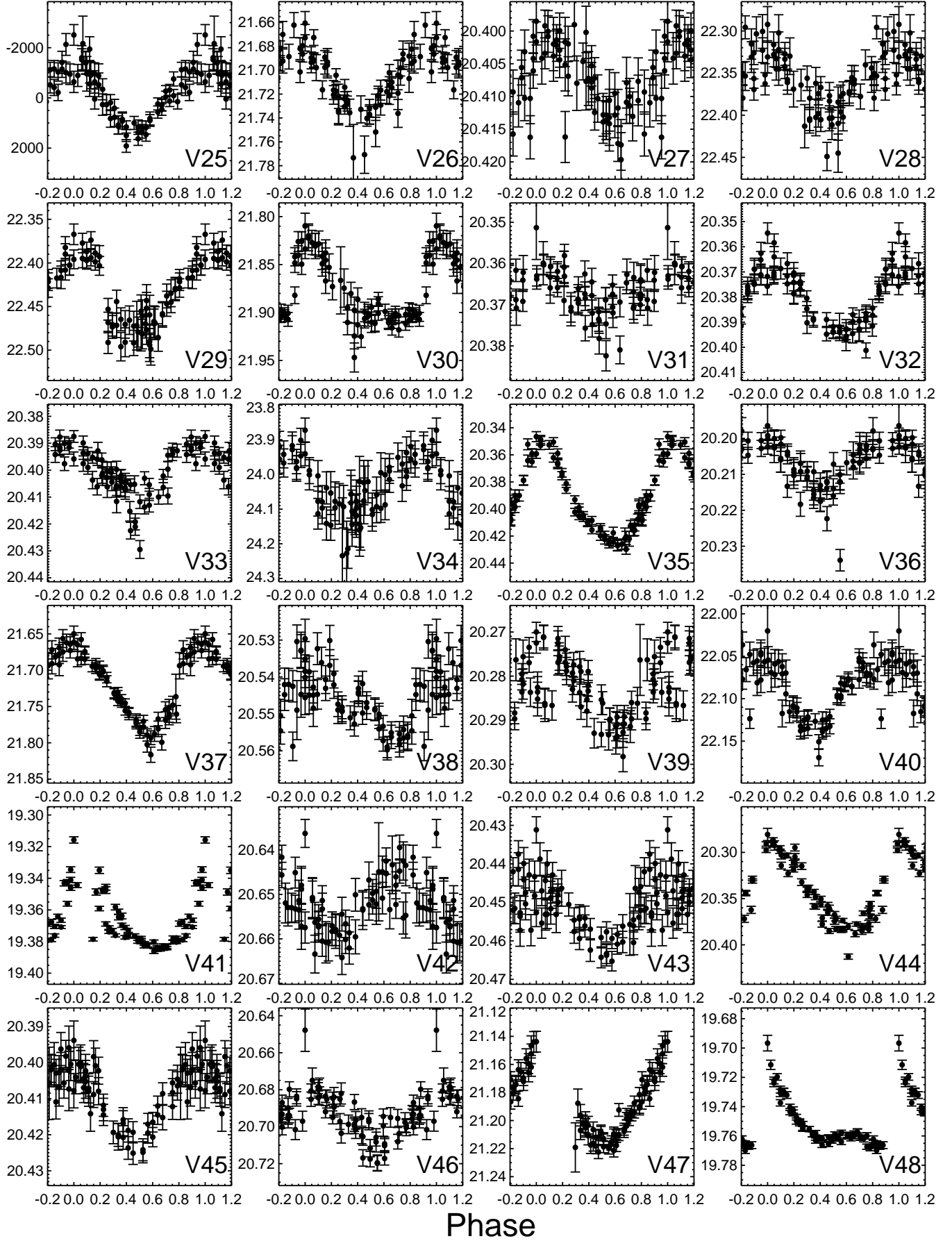


Figure A2. Same as in Fig. A1.

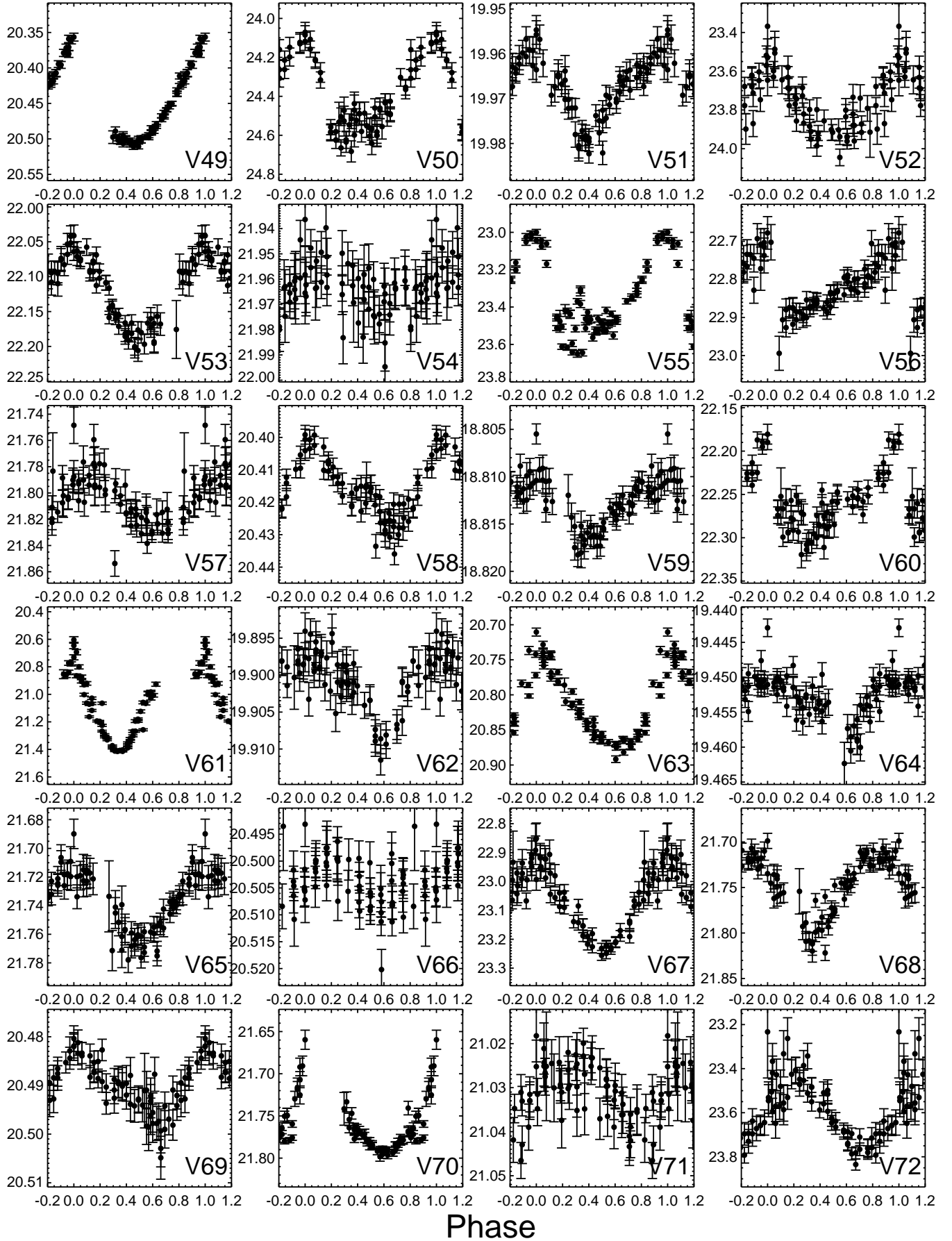


Figure A3. Same as in Fig. A1.

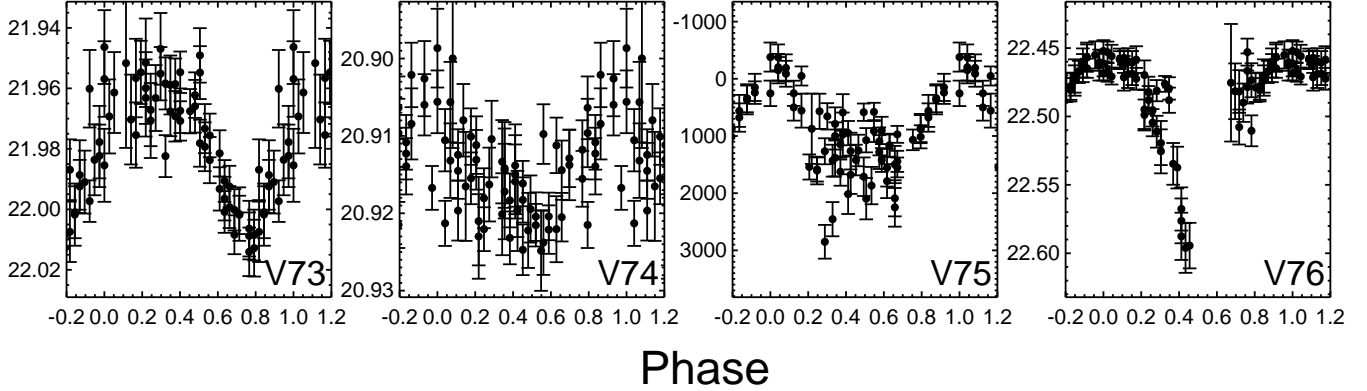


Figure A4. Same as in Fig. A1.

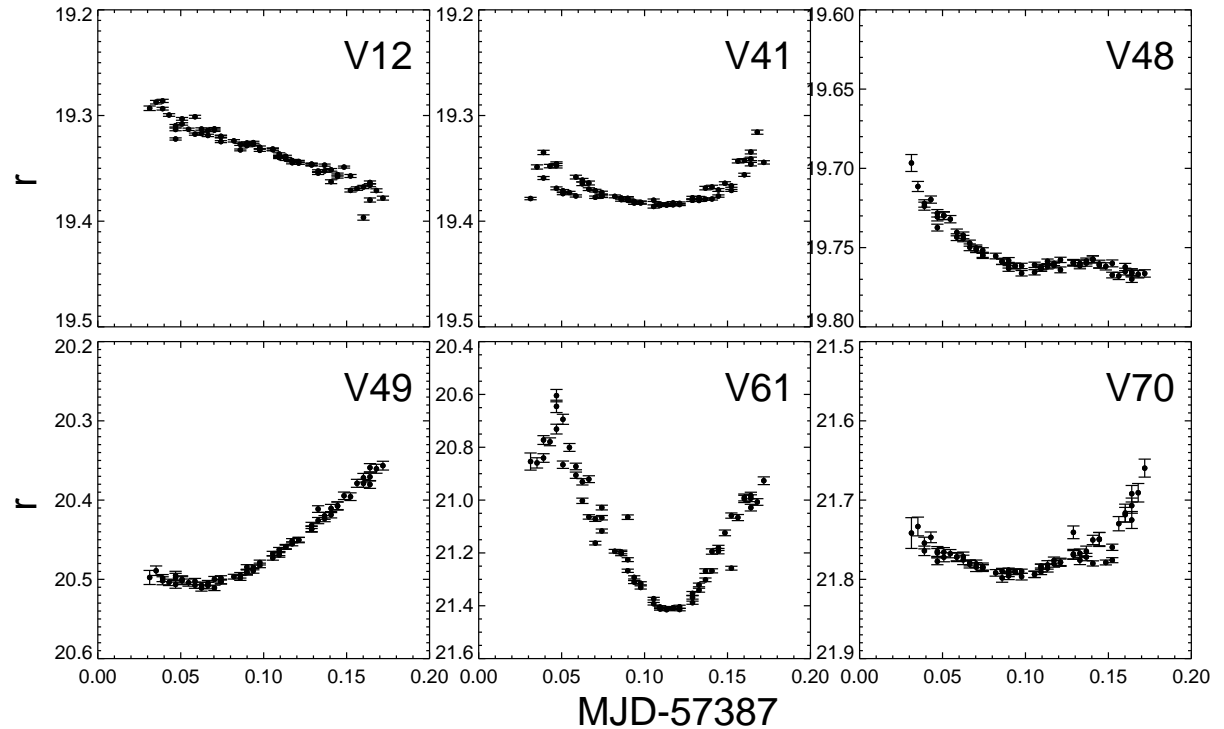


Figure A5. Known RRL (top row) discovered by OGLE and new candidate RRL (bottom row). Light curves are given in modified Julian date versus magnitude.